RSC Advances

NOVEL HYBRID CHITOSAN BLENDED MoO3-TiO2 NANOCOMPOSITE FILM: EVALUATION OF ITS SOLAR LIGHT PHOTOCATLYTIC AND ANTIBACTERIAL ACTIVITY

Journal:	*RSC Advances*
Manuscript ID:	RA-ART-03-2015-005692.R1
Article Type:	Paper
Date Submitted by the Author:	27-Apr-2015
Complete List of Authors:	Paramanandham, Magesan; Anna University, Chemistry Srithar, Sanuja; Anna University, Chemistry Umapathy, Manickam; Anna University, Chemistry

NOVEL HYBRID CHITOSAN BLENDED MoO_3-TiO_2 NANOCOMPOSITE FILM: EVALUATION OF ITS SOLAR LIGHT PHOTOCATLYTIC AND ANTIBACTERIAL ACTIVITY

P. Magesan, S. Sanuja and M. J. Umapathy*

***Corresponding author: Department of Chemistry, College of Engineering Guindy Campus, AnnaUniversity, Chennai - 25, India.**

Abstract

In the present study, we report newly synthesized, TiO_2 and MoO_3-TiO_2 nanocomposites, chitosan and chitosan-blended MoO_3-TiO_2 nanocomposite film by sol-gel and solution cast method, respectively. The synthesized nanocomposite films were characterized by XRD, FT-IR, TG-DTA and FESEM with EDAX. The antibacterial activities for the prepared nanocomposite films were tested against *E.coli* by using well diffusion method.The photocatalytic activities of the materials were investigated against methyl orange dye as a model organic pollutant under the irradiation of solar light. Further, the mechanical properties (Tensile strength and Elongation) were determined using Universal Testing Machine. From the obtained results, it was concluded that the Chitosan-blended MoO_3-TiO_2 nanocomposite film exhibits higher photocatalytic, antibacterial and mechanical properties than the others.

Keywords: Chitosan, MoO_3-TiO_2, Chitosan-blended MoO_3-TiO_2, solar light, photocatalytic activity, antibacterial activity, mechanical properties.

Corresponding author: Tel.: +91-44-22358669, Email address: mj_umapathy@yahoo.co.in

Introduction

In the recent years, the ecological glitches associated to the pollution of water source have gained a lot of attention towards the natural bodies. One of the main sources for the contamination of water pollution is from the textile industries. Because the textile dyeing industries consume large quantities of water and produces large volume of waste water from different steps in the dyeing and finishing process. The worldwide dye consumption for dyeing industries are around 10^7 kg/year.[1] Since the dyes are stable, recalcitrant, colorant and even potentially carcinogenic and toxic, their release into the environment causes a major threats to the environment.[2] The dye contaminated waste water cannot be easily treated because of the natural biodegradability has become increasingly difficult task to the improved properties of dyestuffs. A wide range of conventional methodologies have been used to eliminate these pollutants from the waste water but the efficiency was limited. The modern nanotechnologies have become popular for the fabrication of desirable nanomaterials with large surface-to-volume ratios of unique surface properties to treat these pollutants. Nanoparticles are the key to nanotechnology; hence in-depth study of nanomaterials is an important source for producing new principles, techniques and methods.[3]From environmental standpoint, heterogeneous photocatalysis is an important pioneering technology for application in water purification. With advent of nanotechnology, semiconductor nanoparticles have attracted much intention due to their novel optical, electrical and mechanical properties. Among the various semiconductor nanoparticles, nanosized titanium dioxide (TiO_2) particles are the most frequently studied in the field of solar energy conversion, photocatalysis, transparent UV protection films and chemical sensors etc.,. It has been proved to be one of the most suitable materials in environmental remediation process due to its powerful oxidation strength, low cost, non-toxicity and chemical

stability against photo-corossion.[4-6] However, the conventional TiO_2 photocatalyst suffered an obstacle when applied in practical applications such as effective utilization of UV/solar light, large surface area requirement for the adsorption of pollutant, that is, adverse recombination of electron and holes. Many efforts have been made to extend the adsorption of light from UV to visible region and to improve the photocatalytic efficiency of TiO_2.[7] Enhancing the rate of photoreduction by doping a semiconductor with metal ions can produce a photocatalyst with an improved trapping-to-recombination rate ratio. However, when metal ions or oxides are incorporated into TiO_2 by doping, the impurity energy levels formed in the band gap of TiO_2 can also lead to an increase in the rate of recombination between photogenerated electrons and holes. Photocatalytic reactions can only occur if the trapped electron and hole are transferred to the surface of the photocatalyst. This means that metal ions should be doped near the surface of the photocatalyst to allow efficient charge transfer. Dopants like transition metals (Fe, Al, Ni, Cr, Co, W, V and Zr) and metal oxides (Fe_2O_3, Cr_2O_3, CoO_2, SiO_2, etc.,) being used to improve its applicability.[8-10] The absorption threshold of TiO_2 nanopowder has been shifted from UV to visible region by doping the visible light active material and the photocatalytic efficiencies can be higher than the pure TiO_2 and Degussa P25.[11-14]As a wide band gap n-type semiconductor, Molybdenum oxide (MoO_3) is a potential material because of its wide range of stoichiometry and interesting behavior which includes chemical,[15] structural,[16] electrical and optical[17] properties. With surface modification with MoO_3, the TiO_2 nanoparticles become much more hydrophilic, and they can be more stably suspended in aqueous solution and it is believed that an excellent dispersibility in aqueous solution originates from the high hydrophilicity of MoO_3.[18] The addition of MoO_3 to TiO_2 showed high activity for the photodegradation of molasses and the MoO_3-TiO_2 material has an increased surface area compared to the pure oxides. The modified

material has a reduced band gap and can absorb more light in the near-visible region and thus accelerate the rate of decomposition.[19]

Over the recent years, hybrid materials based on chitosan have been developed, including conducting polymers, metal nanoparticles and oxide agents due to excellent properties of individual components and outstanding synergistic effects simultaneously.[20]In this regard, Chitosan, a linear cationic, pH sensitive, non-toxic, biodegradable and biocompatible polysaccharide prepared from the deacetylation of chitin seems to offer numerous distinct advantages.[21] It is the second most abundant biopolymer widely present as the basic components of exoskeletons of crustaceans and insects. The structure of chitosan is similar to that of cellulose; it consists of β (1-4)-linked D-Glucosamine residue with 2-hydroxyl group being substituted by an amino or acetylated amino group. The structures of cellulose, chitin and chitosan are shown in the figure 1. Chitosan is soluble in diverse acids and able to interact with polyanions to form complexes and gels.It has the adsorption capacity of 1000-1100 g Kg^{-15} which is higher than activated carbon, that is, it is a super high-capacity adsorbent for contaminant removal in water.[22] This high adsorption capacity of chitosan gives rise to the binding ability of chitosan with contaminants in water through hydroxyl and amino groups present on the surface. Currently, researchers have been devoted to fabricate the combination of chitosan and metal oxide nanomaterials for the environmental remediation process. The objective of this study is focused on (i) synthesis and characterization of TiO_2 and MoO_3-TiO_2 nanocomposites, chitosan and Chitosan-blended MoO_3-TiO_2 nanocomposite film by sol-gel and solution cast method, respectively, (ii) photocatalytic activities of the prepared nanocomposites and films towards the degradation of methyl orange dye under the illumination of solar light, (iii) antimicrobial activity of the nanocomposite films were tested against *E.coli* using well diffusion

method, and (iv) further the mechanical properties (Tensile strength and Elongation) were determined using Universal Testing Machine.

2. Experimental details

2.1. Materials

Titanium Tetra IsoPropoxide (TTIP) and Tween-80 were purchased from Spectrochem, Molybdenum trioxide (MoO_3) from SRL. Crab shells were collected from Kasimedu Seafood Market, Sodium hydroxide, hydrochloric acid was purchased from Merck. Glacial acetic acid was obtained from Qualigens were purchased and used as received. Freshly prepared de-ionized water was used in all the experiments.

2.2. Synthesis of MoO_3-TiO_2 and TiO_2 nanocomposites

MoO_3 nanoparticles were suspended in 20 ml of distilled ethanol and stirred for 30 minutes. To the homogeneous dispersion 3 ml of tween-80 was added under stirring and further stirred for 30 minutes. A mixture of 3 ml TTIP with 10 ml isopropyl alcohol was added drop wise into the suspension and the stirring was continued for 2 h to get a gel. The resultant gel was filtered off and washed thoroughly with 1:1aqueous ethanol, filtered and then oven dried at 120 ºC for 6 hrs. The solid sample was calcined at 500 ºC for 3 hrs using an electrical muffle furnace. The similar procedure has been followed for the preparation of TiO_2 nanocomposites without adding MoO_3 nanoparticles.

2.3. Synthesis of Chitosan from Crab shell

The Crab shells were collected from Kasimedu Seafood Market, Chennai, Tamil Nadu, India. The Crabs exoskeletons collected were placed in Ziploc bags and refrigerated overnight. The synthesis of chitosan can be achieved by performing the following four steps;

(i) Coarse purification: Approximately 500 g of crab shells were coarsely cleaned with running water until sand and other impurities like soils were removed. The cleaned crab shells were dried overnight in the hot air oven at 110°C.

(ii) Deproteinization: The dried shell samples were groundedby using a mortar and transferred to a beaker. 2% of NaOH was added to the beaker containing the shell samples and heated under stirring at 60–70 °C for 30 minutes. The shell samples were filtered off with a strainer and the process was repeated for few times until the filtrate become clear and colorless. The samples were washed with demineralized water to remove the unreacted NaOH. For time-saving the shells samples may be soaked in NaOH solution for overnight after first NaOH treatment, again it was filtered and washed.

(iii) Demineralization: 7% of HCl was slowly added to the shells and the mixture was stirred at room temperature until the effervescence. The mixture was filtered off and washed with excess distilled water. The samples were dried overnight in a hot air oven at 60 °C to get around 100 g of chitin was obtained from crab shells. This step was known as demineralization.

(iv) Synthesis of chitosan from chitin by partial deacetylation: Chitin was loaded in a RB flask and 50% NaOH. The samples were heated at 125 °C for 2 h and then allowed to cool down followed by the addition of 250 mL of water. The next day the sample was filtered off and the residue was washed with excess water and dried in the hot air oven at 60 °C for 2 hr.

2.4. Casting of Chitosan film

Chitosan film was synthesized by solution cast method. 1 g of chitosan was dissolved in 100 mL of 1% (v/v) acetic acid solution and allowed to stirring for 24 hours. Later, it was sonicated for 15 min for well dispersion. Further, it was casted in a petri-dish and kept in an oven at 50-60 ºC for overnight to get a homogeneous film.

2.5. Casting of Chitosan-blended MoO_3-TiO_2 nanocomposite film

1 g of prepared MoO_3-TiO_2 composites was added into the chitosan solution (1 g of chitosan in 100 mL of 1% (v/v) acetic acid) and sonicated for 30 minutes and stirred continuously for 12 hrs until the clear solution was obtained. The mixture solution was cast onto the petri plates and dried at room temperature for 48 hrs to obtain the composite film.

2.6. Solar light intensity measurements

Solar light intensity was measured for every 30 min and the average light intensity over the period of an each experiment was calculated. The sensor was always set in the position of maximum intensity. The intensity of solar light was measured using New 200,000 Lux Digital Meter Light Luxmeter Meter Photometer with Footcandle FC. The intensity was 1200 X 100 ± 100 lux and it was nearly constant in the course of the experiments.

2.7. Photocatalytic degradation of Methyl orange dye

The photocatalytic experiments were carried out under identical conditions on sunshiny days between 11 a.m. and 2 p.m. In all experiments, 50 ml of the reaction mixture was irradiated under sunlight. An open borosilicate glass tube of 50 mL capacity, 40 cm height and 20 mm diameter was used as the reaction vessel. The suspensions were

magnetically stirred in the dark for 15 min to attain adsorption–desorption equilibrium between the dyes and TiO_2 and MoO_3-TiO_2 nanocomposites, chitosan and Chitosan-blended MoO_3-TiO_2 nanocomposite film. Irradiation was carried out in the open-air condition. 50 mL of the dye solution with the synthesized catalysts were constantly aired by a pump to provide oxygen and for the thorough mixing of reaction solution. There is no volatility of the solvent was observed during the illumination time. After dark adsorption the first sample was taken. At specific time (15 min) intervals 2–3 mL of the sample was withdrawn and centrifuged to separate the catalyst. 1 mL of the sample was properly diluted and its absorbance at 464 nm was measured immediately to monitor the degradation of the methyl orange.

2.8. Determination of antibacterial activity

The in vitro antibacterial action of the prepared samples was examined using gram negative bacteria (*Escherichia coli* ATCC 25922) by well diffusion method. Nutrient agar was prepared and poured in the sterile Petri dishes and allowed to solidify. 24 h growing bacterial cultures (*E. coli*) were swabbed on it. The 5 wells (10 mm diameter) were made by using cork borer. The four different concentrations (250 µg, 500 µg, 750 µg and 1000 µg) of the nanoparticle, one negative control were loaded in the wells. The plates were then incubated at 37 ºC for 24h. After incubation the inhibition diameter was measured. Percentage of inhibition was calculated by using the formula (Eq. 1)

$$\% \text{ of inhibition} = \left\{ \frac{\text{I (Diameter of the Inhibited Zone)}}{\text{90 (Diameter of the Petri-plate in mm)}} \text{X100} \right\} \quad (1)$$

2.9. Instrumentation and Analysis

The following physiochemical techniques have been used to characterize the prepared catalysts. To characterize the phase structure of the TiO_2 and MoO_3-TiO_2 nanocomposites, chitosan and Chitosan-blended MoO_3-TiO_2 nanocomposite film; a Bruker D2 Phaser Desktop X-ray Diffractometer equipped with Ni-filtered Cu Kα radiation (λ=1.542 Å) and operated at an accelerating voltage and emission current of 30 kV and 10 mA, respectively. Data were acquired over the range of 2θ from 0° to 70 °C with a step size of 0.0017 and a scan rate of 7°/min. Field Emission Scanning Electron Microscopy (FESEM) was performed to examine the surface morphology of the prepared nanocomposites using DXS-10 ACKT scanning electron microscope equipped with EXS, which was used to study the elemental composition. For Fourier transform infrared spectroscopy (FT-IR) analysis, the KBr pellets were prepared from the TiO_2 and MoO_3-TiO_2 nanocomposites, chitosan and Chitosan-blended MoO_3-TiO_2 nanocomposite film. FT-IR analysis was performed using a spectrophotometer (Perkin Elmer RX1 instrument). Thermogravimetric-differential thermal analysis (TG-DTA) of the nanocomposites was taken on WATERS SDT Q 600 TA model instrument. Mechanical properties (Tensile strength and Elongation) of the films were determined according to ASTM standard method with Universal Testing Machine (TNUM-5900). The film was cut into (7x3 cm) rectangular shapes and measured.

3. Results and discussion

3.1. Surface morphology of TiO_2 and MoO_3-TiO_2 nanocomposites, chitosan and Chitosan-blended MoO_3-TiO_2 nanocomposite film

Field Emission Scanning Electron Microscopy (FESEM) was used to investigate the surface morphology of the prepared chitosan film, TiO_2, MoO_3-TiO_2, Chitosan-blended MoO_3-TiO_2 composite film. The FESEM pictures of chitosan, TiO_2, MoO_3-TiO_2 nanocomposites and Chitosan-blended MoO_3-TiO_2 nanocomposite film are shown in the Fig 2 (a-d), respectively. The chitosan, TiO_2, MoO_3-TiO_2 and chitosan-blended MoO_3-TiO_2 composite film has aggregated particle structure with almost spherical morphology. But at the same time, TiO_2 and MoO_3-TiO_2 nanocomposites reveal the agglomeration of the nanoparticles which may be due to the presence of templating agent. As can be seen in the Fig. 2d, it is noteworthy that the chitosan particles are non-uniformly mixed in the MoO_3-TiO_2 matrix.

3.2. Elemental composition

The elemental compositions of the TiO_2 and MoO_3-TiO_2 nanocomposites and Chitosan-blended MoO_3-TiO_2 nanocomposite film were studied by Energy Dispersive Analysis of X-rays (EDAX). Figure 3 (a-c) depicts the EDAX analysis of the TiO_2, MoO_3-TiO_2 and chitosan-blended MoO_3-TiO_2 composite film, respectively from a selected areain the binding region of 0-10 keV. The signals from the spectra reveal the presence of Ti, O, Mo and C in the prepared nanocomposites. The result corroborates the formation of chitosan-MoO_3-TiO_2 nanocomposite film.

3.3. Crystalline phases

The crystalline phases of the prepared TiO_2 and MoO_3-TiO_2 nanocomposites, chitosan and Chitosan-blended MoO_3-TiO_2 nanocomposite film were studied by X-Ray Diffraction analysis. Figure 4 depicts the XRD pattern of the prepared nanocomposites. In TiO_2, MoO_3-TiO_2 and chitosan-blended MoO_3-TiO_2 composite film, TiO_2 exists in anatase phase show their sharp characteristic peaks at 2θ= 25.3°, 37.8°, 48.1°, 54.0°, 55.1°, 62.8° and 75.0° corresponds to the (101), (004), (200), (105), (211), (204) and (215) planes agree well to standard JCPDS card No. 89-4921 and hence confirms that the nanocomposite have been predominantly crystalline in nature with anatase phase. There is no characteristic peaks of MoO_3 has been observed and hence it can be established that doping of MoO_3 did not influence the crystal structure of the TiO_2 particles. It was clear that the chitosan is highly crystalline in nature and shows the characteristics peaks at 2θ= 9.2°, 19.2°, 26.9°, 34.9°, 38.8°, 43.5°, 51.0° and 72.8°, which suggests the formation of inter- and intra-molecular hydrogen bonds in the presence of free amino groups in the chitosan. The average crystallite sizes of the nanocomposites have been deduced from the half-width of the full maximum (HWFM) of the most intense peak using Scherrer equation (Eq. 2),

$$t = K\lambda/\beta\cos\theta, \quad (2)$$

Where t is the crystallite size, K is the shape factor of value 0.9, λ is the wavelength of the X-ray used. θis the Bragg's diffraction angle, β is the corrected line broadening, $\beta = \beta_b - \beta_s$, β_b is the broadened profile width of the experimental sample and β_s is the standard profile width of the reference (high purity silica) sample. According to the Eq. 2, the average crystallite sizes of the prepared samples are listed in the table 1.

3.4. Fourier Transform Infrared Spectroscopy (FTIR)

FTIR spectrum provides information on the nature of the synthesized nanocomposites. FTIR spectra of TiO_2 and MoO_3-TiO_2 nanocomposites, chitosan and Chitosan-blended MoO_3-TiO_2 nanocomposite film were presented in the figure 5. For chitosan and chitosan-blended MoO_3-TiO_2 composite film spectrum (Fig. 5 c &d), shows absorption peak at 3423-3500 cm^{-1} and 1643-1647 cm^{-1}, which are attributed to the amine ($-NH_2$) and hydroxyl (-OH) functional groups, respectively.[23] Both of these functional groups on chitosan chain can serve as coordination and reaction sites for the adsorption of the organic species.[24] Fig. 5 (a,b&d) also confirms the existence of metal oxide (TiO_2) peak around 742-783 cm^{-1} for TiO_2, MoO_3-TiO_2 and chitosan-blended MoO_3-TiO_2 composite film. A weak band at around 2340-2370 cm^{-1} may be attributed to the vibrations of atmospheric CO_2. The apparent existence of amine or amide and hydroxyl functional groups together with metal oxides should help to confirm the effective removal of the organic dyes through photodegradation-adsorption process.[25]

3.5. TG-DTA Analysis

TG-DTA analysis was carried out to study the thermal decomposition behavior of the synthesized TiO_2 and MoO_3-TiO_2 nanocomposites, chitosan and Chitosan-blended MoO_3-TiO_2 nanocomposite film are shown in the figure 6. The synthesized chitosan film shows two weight loss curves, first stage of weight loss was due to evaporation of water and the second stage of weight loss was due to the degradation of the polymer chain. In TGA of TiO_2, three noticeable steps observed, which are in the range of 200- 340 °C, 341- 400 °C and 500 - 585 °C. The TGA curve shows two exothermic peaks and the first

exothermic peak with a maximum of 282 °C, sharp and narrow and this may be attributed to the burnout of the templating agent. The second weak exothermic peak corresponds to the crystallization process of TiO_2 with a maximum of 354 °C.[26] In TG-DTA curve of MoO_3-TiO_2, two main exothermic peaks has been found, the larger peak centered around 363 °C and sharp peak centered around 401 °C. This may be attributed to the burnout of the surfactant template and crystallization process, respectively. In chitosan-blended MoO_3-TiO_2 film, three weight losses were observed. At 100 °C, first weight loss was observed which was due to the evaporation of water and the second weight loss around 150 °C was due to polymer degradation and the last and final weight loss at 400 °C was The weight loss at 400 °C may be due to the decomposition of organic matter and the compound remain stable.

3.6. Photocatalytic activity

For the efficient use of solar light or use of the visible region of the spectrum, the technologies expanding the absorption scope of TiO_2 may then give the impression as an attractive challenge for developing the future generation of photocatalysts.[27] The visible light photocatalytic activity of the F- doped TiO_2 was achieved by creating the oxygen vacancies.[28] Bismuth oxohalide nanoplates on TiO_2 nanoribbons as sunlight-driven bifunctional photocatalysts for all-weather removal of pollutants. BiOBr@TiO_2 framework exhibits very impressive sunlight-driven photocatalytic activity, which is much higher than commercially available P25 TiO_2 under the same conditions.[29] The photocatalytic activity of the TiO_2 and MoO_3-TiO_2 nanocomposites, chitosan and Chitosan-blended MoO_3-TiO_2 nanocomposite film was investigated by the photodegradation of the methyl orange dye (model organic pollutant) over a period of 2

hour under solar light irradiation. Percentage removal was calculated by using the following equation (Eq. 3)

$$\% \text{ removal of model pollutant} = \frac{Co - Ct}{Co} \times 100 \quad (3)$$

Where, Co = concentration of model pollutant at 0 min, Ct = concentration of model pollutant at experimental time, t.

The photocatalytic mechanism was as follows: when the synthesized nanoparticles were illuminated under solar light irradiation, the electron transition from the valence band (VB) to the conduction band (CB) resulting in the electron (e^-)- hole (h^+) pair in which the electron (e^-) was getting reductive, and the hole (h^+) was oxidative and the general photocatalytic mechanism is shown in the figure 7. The hole (h^+) reacted with OH^- on the surface of the nanomaterials, generating hydroxyl radicals ($^{\bullet}OH$), superoxide anion (O_2^{-}) and perhydroxyl radicals (HO_2^-). The ·OH radicals are extraordinarily reactive species and attack most of the organic molecules with rate constants usually in the order of 10^6 - 10^9 M^{-1} s^{-1}. Figure 8 displays the photodegradation profiles of methyl orange dye by the synthesized nanocomposites. It can be seen from the figure 8, that all of the samples were capable of degrading methyl orange as indicated by the decrease in the methyl orange solution concentration throughout the period of the photocatalytic study but the TiO_2 has almost no photocatalytic activityunder identical conditions. Besides, the photocatalytic activity increased in the order TiO_2 < MoO_3-TiO_2 < Chitosan film < Chitosan-blended MoO_3-TiO_2 composite film. Hence, Chitosan-blended MoO_3-TiO_2 exhibits highest photocatalytic activity among the investigated catalysts in the photodegradation of methyl orange. Generally, the photocatalytic activity of the catalyst is influenced by various

factors, particularly by light harvest, charge separation efficacy and the adsorption ability to target pollutants. So, the high photocatalytic activity of Chitosan-blended MoO_3-TiO_2 composite film compared with pure TiO_2 under solar light irradiation was attributed to the transfer and separation of photo-generated charge among the respective energy levels of the semiconductor photocatalyst. The photocatalytic studies show that the introduction of CNTs into TiO_2 nanofiber membranes facilitated the separation of the photo-generated charges, leading to an enhancement of the photocatalytic activity toward the decomposing Methylene blue (MB) in water under the illumination of solar light.[30] The recyclability experiments were performed are shown in the figure 9. After each experiment, the photocatalyst was washed thrice with ethanol, filtered, dried at 70 °C and reused. The catalysts showed some favorable reusability after 4 times of recycling. But we did observe some extent of loss in the catalytic activity after each cycle. The decrease in the degradation rate may be due to the weakening of the absorbance ability or the loss of some catalyst during the collection of the catalysts.

3.8. Antimicrobial activity

The antimicrobial activity of synthesized Chitosan-blended MoO_3-TiO_2 film (A), MoO_3-TiO_2 (B), TiO_2 (C) and chitosan film (D) were examined by well diffusion method against the bacteria *E.Coli*. The samples were tested by using four different concentrations such as 250 μg, 500 μg, 750 μg and 1000 μg. The zones of inhibition of the synthesized samples against *E. coli* for the various concentrations are displayed in the table 1 and the corresponding bar diagram is shown in the figure 10. From the results of zone of inhibition method (Figure 11), it was observed that all the samples have no activity at 250 μg concentration. At 500 μg, Chitosan-blended MoO_3-TiO_2 and chitosan

film has 10 mm and 9 mm zone of inhibition, respectively, while MoO_3-TiO_2 and TiO_2 never showed any activity, this is because of the presence of chitosan which possessed good anti-bacterial activity. At 750 μg, Chitosan-blended MoO_3-TiO_2 film, MoO_3-TiO_2 and chitosan film showed 12, 9 and 10 mm of zone of inhibition while TiO_2 never showed any activity even at this concentration. As we increase the concentration higher to 1000 μg the activity increases up to 13 mm and 11 mm for Chitosan-blended MoO_3-TiO_2 film, MoO_3-TiO_2 and chitosan film, respectively, nevertheless TiO_2 does not show any activity. From the results obtained it was confirmed the presence of chitosan increases the activity by increasing the concentration while TiO_2 doesn't show any antibacterial activity for all the four concentrations and remains inactive in the dark condition.

3.9. Mechanical property

Mechanical studies of the synthesized chitosan film and chitosan- blended MoO_3-TiO_2 films were carried out, through which their tensile strength and elongation were measured and shown in the figure 12. Pure chitosan film has low tensile strength of 65 MPa when compared to chitosan-MoO_3-TiO_2 film whose strength was found to be 76 MPa. Nanoparticle doped chitosan film has higher strength due to the strong interaction of nanoparticles and the NH_2 group present in the chitosan molecules. Elongation of the films were found in which chitosan film has low elongation of 10% while MoO_3-TiO_2 doped chitosan film has high elongation of 28 % because of the well dispersion of metal oxide into the polymer film.

Conclusions

In summary, a kind of novel chitosan-blended MoO_3-TiO_2 nanocomposite film, chitosan film, MoO_3-TiO_2 and TiO_2 nanocomposites were prepared by a simple method. The synthesized materials were characterized by XRD, FT-IR, TG-DTA and FESEM with EDAX. Among the synthesized materials, Chitosan-blended MoO_3-TiO_2 nanocomposite film exhibits higher photocatalytic, antibacterial and mechanical properties. It is cost effective and environment-friendly materials for engineering applications for the removal of contaminants in water from the textile industries.

Acknowledgements

P. Magesan is thankful to University Grants Commission, Delhi for the financial support and we thank the DST-FIST, Department of Chemistry, College of Engineering Guindy Campus, Anna University, Chennai, India for providing lab and instrument facilities for this research work.

References

[1] Y.C. Wong, Y.S. Szeto, W.H. Cheung and G. McKay, *Process Biochem.,* 2004, 39, 693.

[2] G. Moussavi and M. Mahmoudi, *J. Hazard. Mater.,* 2009, 168, 806.

[3] C. Burda, X.B. Chen, R. Narayanan, and M.A. El-Sayed, *Chem. Rev.,* 2005, 105, 1025.

[4] A. Nakajima, H. Obata, Y. Kameshima and K. Obata *Catal. Commun.*, 2005, 6, 716.

[5] Q.J. Xiang, K.L. Lv and J.G. Yu, *Appl. Catal. B,* 2010, 96, 557.

[6] T.Y. Leung, C.Y. Chan, C. Hu, J.C. Yu and P.K. Wong, *Water Res.,* 42, 2008, 4827.

[7] M.A. Rauf, M.A. Meetani and S. Hisaindee, *Desalination,* 2011, 276, 13.

[8] H.K. Shon, D.L. Cho, S.H. Na, J.B. Kim, H.J. Park and J.H. Kim, *J. Ind. Eng. Chem.,* 2009 15, 476.

[9] S. Chang and W. Liu, *App. Catal. B: Environ.* 2011, 101, 333.

[10] N. Venkatachalam, M. Palanichamy, B. Arabindoo and V. Murugesan, *J. Mol. Catal. A: Chem.*, 2007, 266, 158.

[11] M.S. Nahar, K. Hasegawa, S. Kagaya and S. Kuroda, *Sci. Technol. Adv. Mater.,* 2007, 8 286.

[12] T.K. Ghorai, S.K. Biswas and P. Pramanik, *Appl. Surf. Sci.,* 2008, 254, 7498.

[13] N.D. Abazovic, L. Mirenghi, I.A. Jankovic, N. Bibic, D.V. Sojic, B.F. Abramovic and M.I. Comor, *Nanoscale Res. Lett.,* 2009, 4, 518.

[14] C.L. Luu, Q.T. Nguyen and S.T. Ho, *Adv. Nat. Sci. Nanosci.: Nanotechnol.*, 2010, 1, 01.

[15] Y. Shi, B. Guo, S. A. Corr, Q. Shi, Y. S. Hu, K. R. Heier, L. Chen, R. Seshadri and G. D. Stucky , *Nanolett.,* 2009, 9, 4215.

[16] D. Parviz, M. Kazemeini, A.M. Rashi and K.J. Jozani, *J. Nanopart. Res.,* 2010, 12, 1509.

[17] Y. Zhao, J. Liu, Y. Zhou, Z. Zhang, Y. Xu, H. Naramoto and S. Yamamoto, *J. Phys. Cond. Matter.,* 2003, 15, 547.

[18] K. Y. Song, M. K. Park, Y. T. Kwon, H. W. Lee, W. J. Chung and W. I. Lee, *Chem. Mater.,* 2001, 13, 2349.

[19] M. Navgire, A. Yelwande, D. Tayde, B. Arbad and M. Lande, *J. Compos. Mater.,* 2012, 33, 261.

[20] L. H. Li, J. C. Deng, H. R. Deng, Z. L. Liu, and L. Xin, *Carbohydr. Res.*, 345, 2010, 994.

[21] E.I. Rabea, M.E.T. Badawy, C.V. Stevens, G. Smagghe, and W. Steurbaut, *Biomacromolecules*, 2003, 4, 1457.

[22] Z.Y. Liu, H.W. Bai, and D.D. Sun, *New J. Chem.,* 2011, 35, 137.

[23] O.A.C. Monteiro and C. Airoldi, *J. Colloid Interface Sci.,* 1999, 212, 212.

[24] F.C. Wu, R.L. Tseng and R.S. Juang, *J. Hazard. Mater.,* 2001, 81, 167.

[25] Z. Zainal, L. K. Hui, M. Z. Hussein, A. H. Abdullah and I. R. Hamadneh, *J. Hazard. Mater.,* 2009, 164, 138.

[26] Q. Dai, L.Y. Shi, Y.G. Lu, J.L. Blin, D.J. Li and C.W. Yuan, *J. Photochem. Photobiol. A*, 2002, 148, 295.

[27] J. Xu, Y. Ao, D. Fu and C. Yuan, *Appl. Surf. Sci.,* 254, 2008, 3033.

[28] D. Li, H. Haneda, N. K. Labhsetwar, S. Hishita and N. Ohashi, *Chem. Phys. Lett*., 401, 2005, 579.

[29] X. Cao, Z. Lu, L. Zhu, L. Yang, L. Gu, L. Caia and J. Chena, *Nanoscale*, 6, 2014, 1434.

[30] L.W. Zhu, L. K. Zhou, H.X. Li, H.F. Wang and J.P. Lang, *Mater. Lett.,* 95, 2019, 13.

Table 1 Average Crystallite Size (T) obtained from XRD analysis and Zone of inhibition of TiO_2 and MoO_3-TiO_2 nanocomposites, chitosan and chitosan-blended MoO_3-TiO_2 nanocomposite film against E. coli

S. No.	Nanocomposites	T, nm	Zone of inhibition, mm			
			250 µg	500 µg	750 µg	1000 µg
1	TiO_2	12	NA	NA	NA	NA
2	MoO_3 - TiO_2	11	NA	NA	9	11
3	Chitosan film	16	NA	9	10	11
4	Chitosan-blended MoO_3 - TiO_2 film	17	NA	10	12	13

***NA- Non-Active**

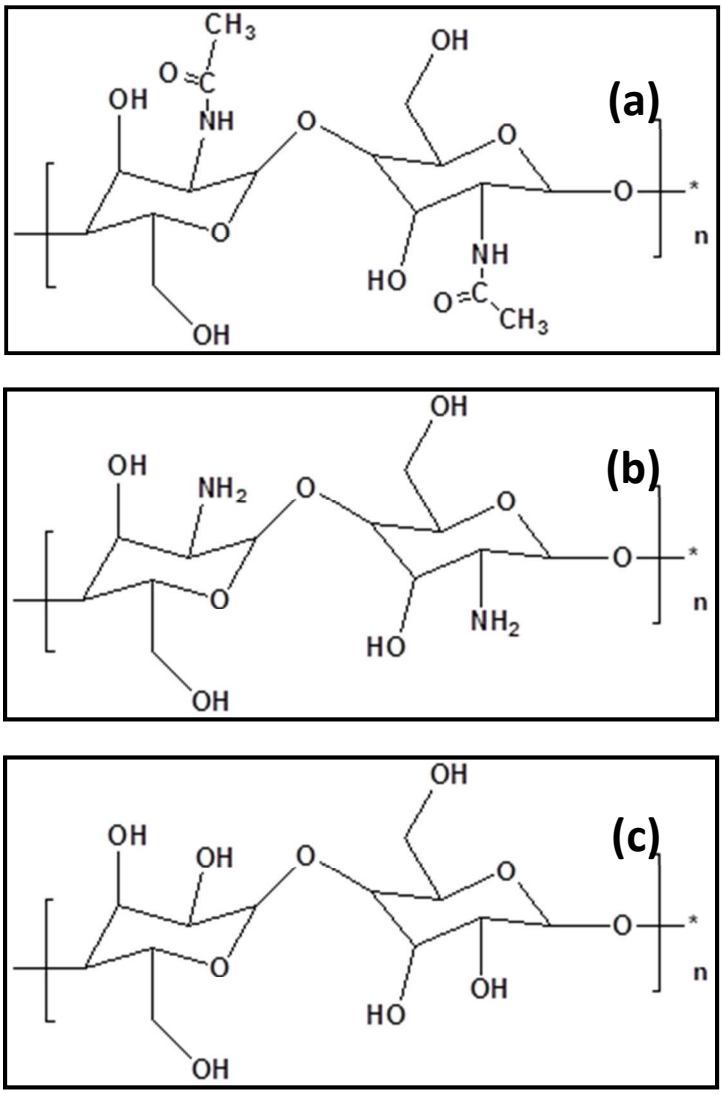

Fig. 1. Comparison of (a) Chitin (b) Chitosan and (c) Cellulose formulae

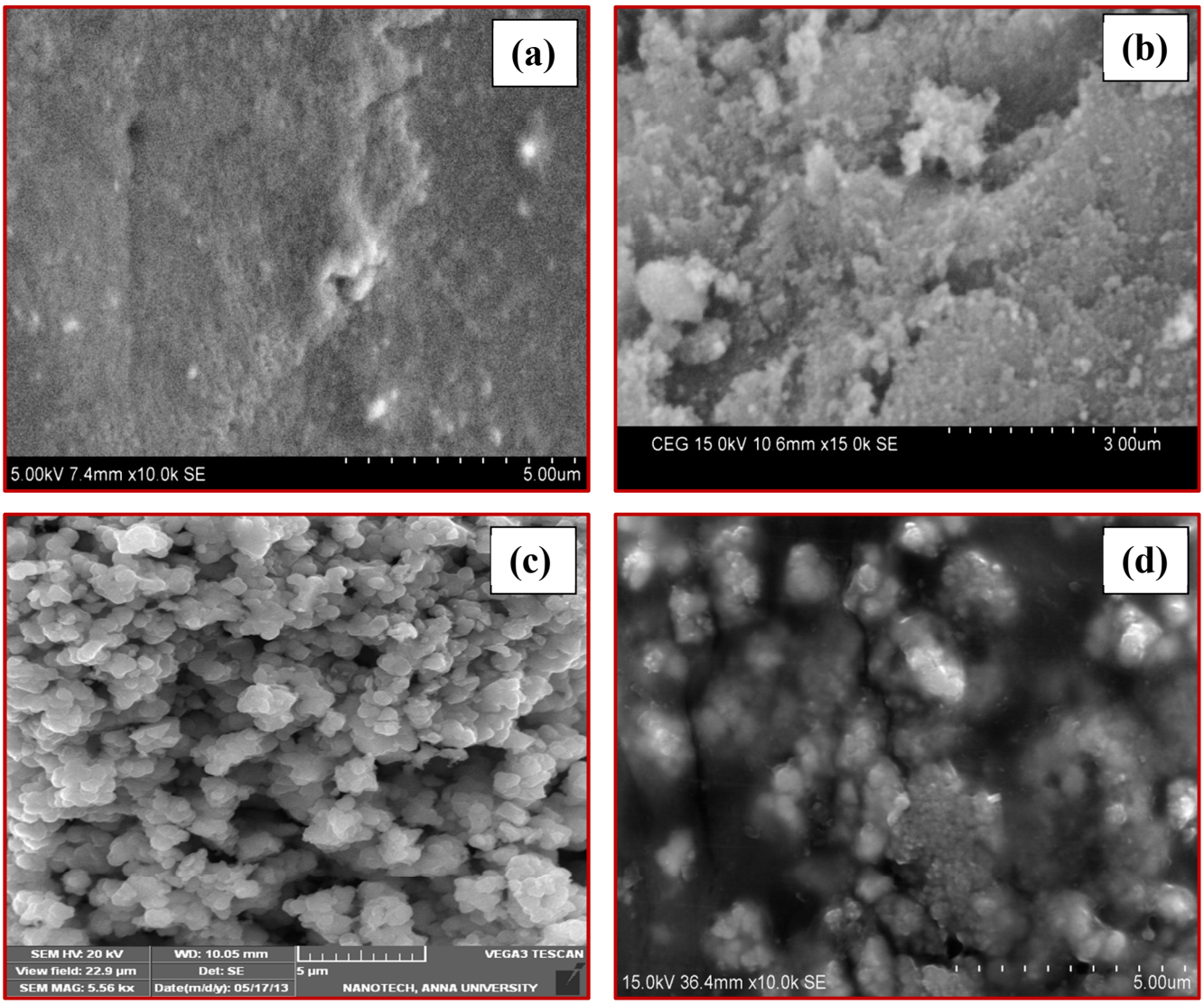

Fig. 2. FESEM micrographs of (a) Chitosan film, (b) TiO_2, (c) MoO_3-TiO_2 and (d) Chitosan-blended MoO_3-TiO_2 film

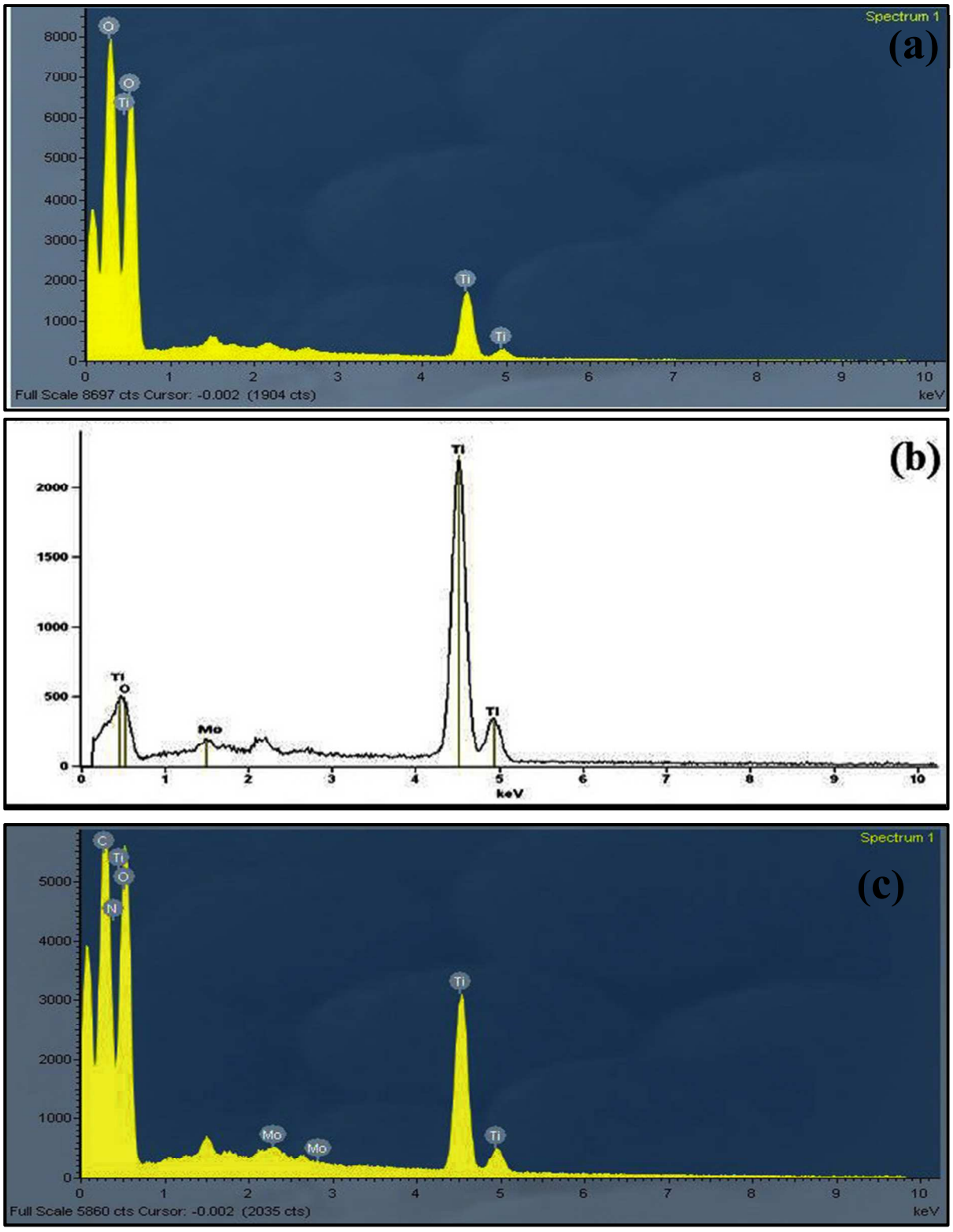

Fig. 3. EDX spectra of (a) TiO_2, (b) MoO_3-TiO_2 and (c) Chitosan-blended MoO_3-TiO_2

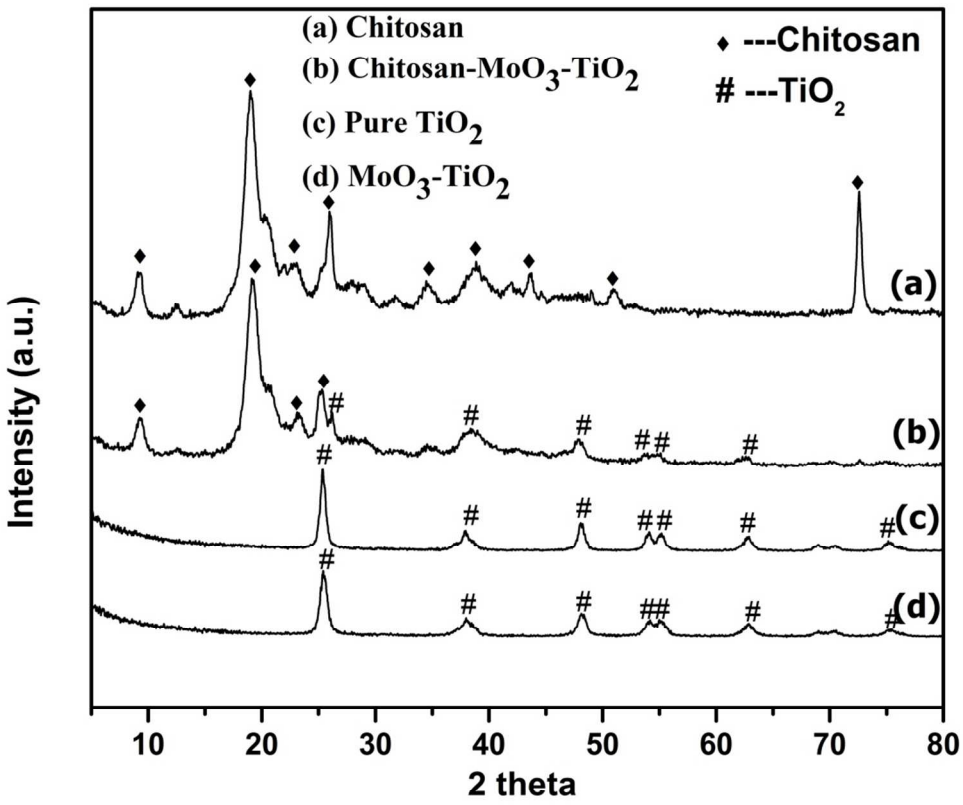

Fig. 4. XRD patterns of (a) Chitosan film, (b) Chitosan-blended MoO_3-TiO_2, (c) TiO_2 and (d) MoO_3-TiO_2

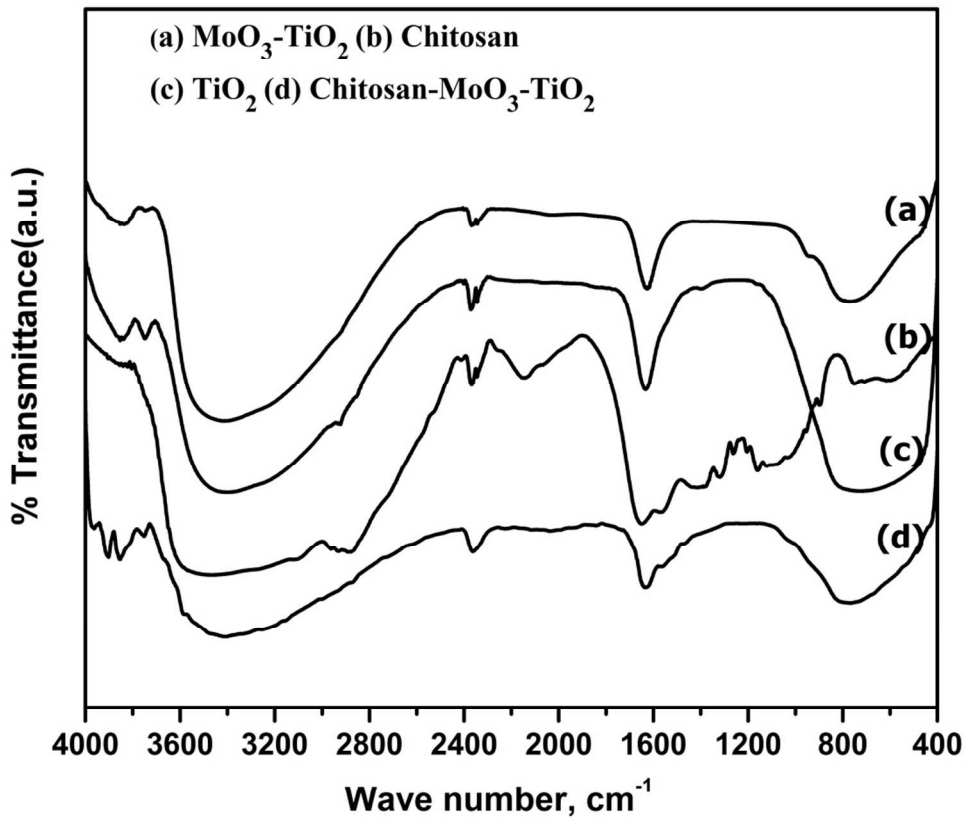

Fig. 5. FTIR spectra of (a) MoO_3-TiO_2, (b) Chitosan film, (c) TiO_2 and (d) Chitosan-blended MoO_3-TiO_2

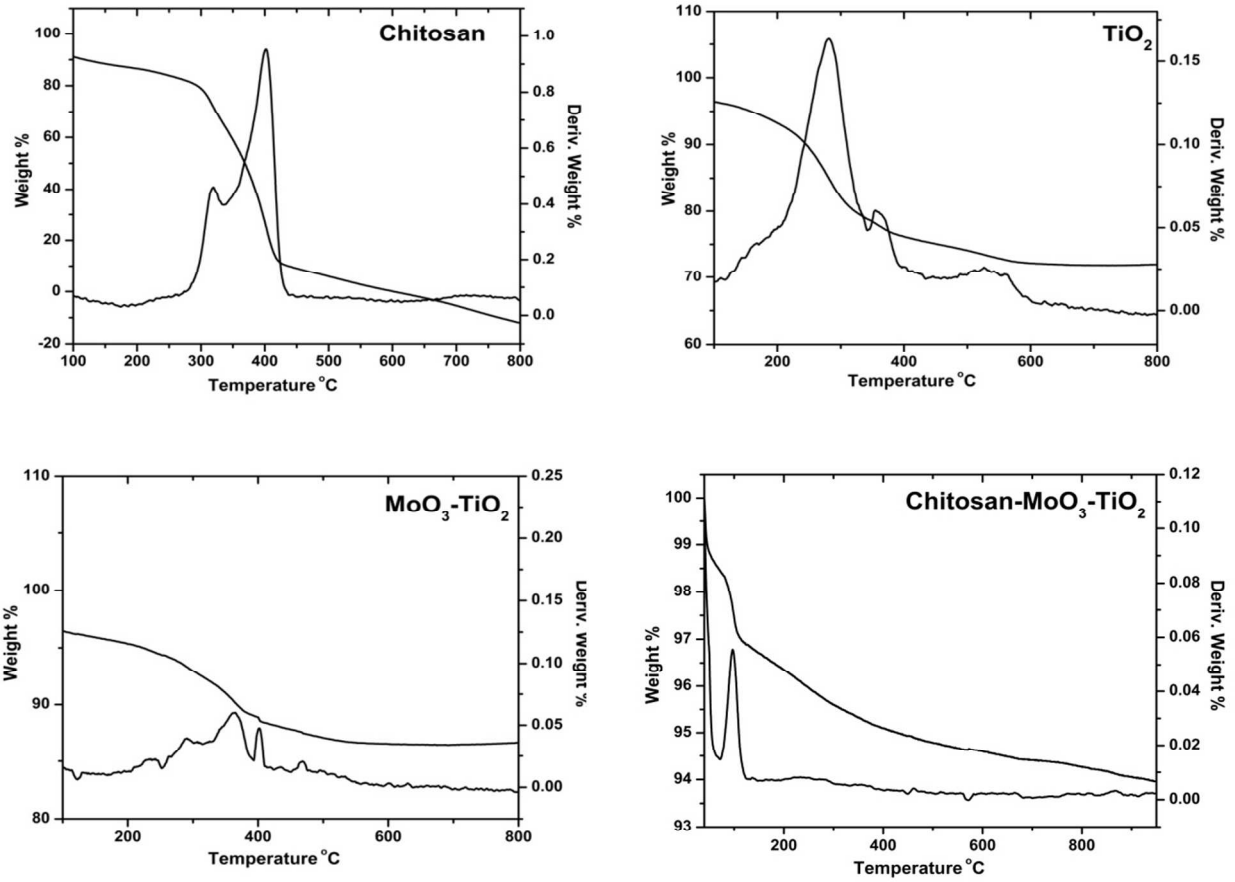

Fig. 6. TG-DTA of Chitosan film, TiO_2, MoO_3-TiO_2 and Chitosan-blended MoO_3-TiO_2

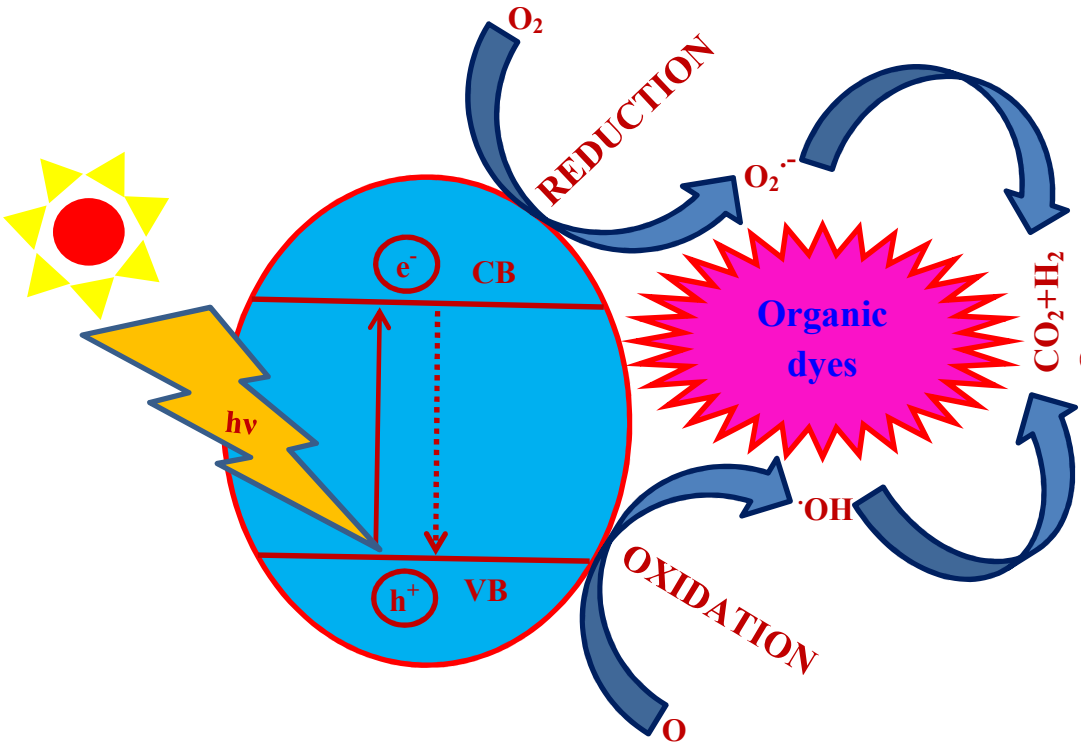

Fig. 7. General Photocatalytic mechanism

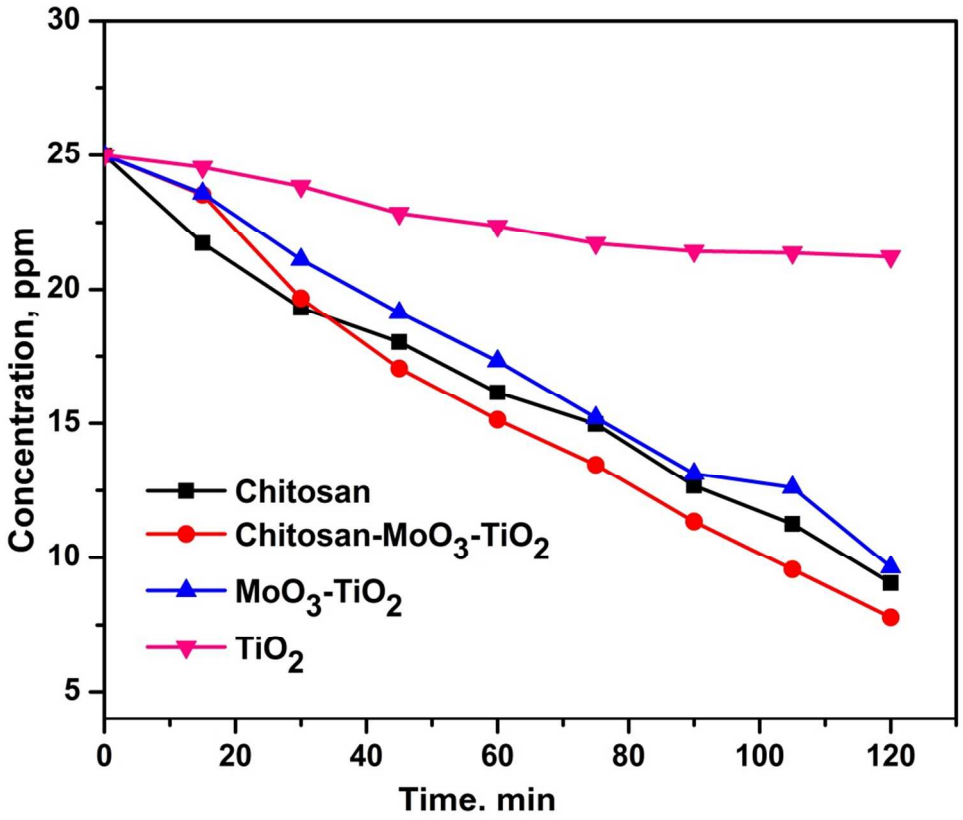

Fig. 8. Solar light photodegradation profiles of Methyl orange dye

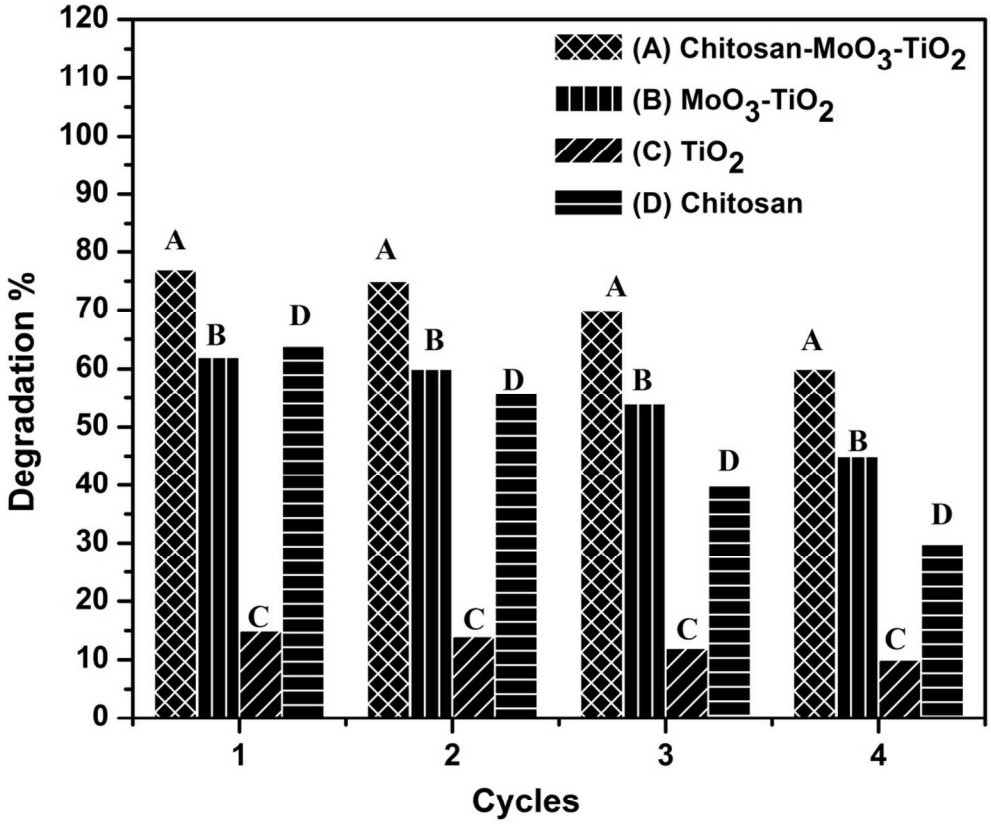

Fig. 9. Recyclability degradation percentage of the prepared composites

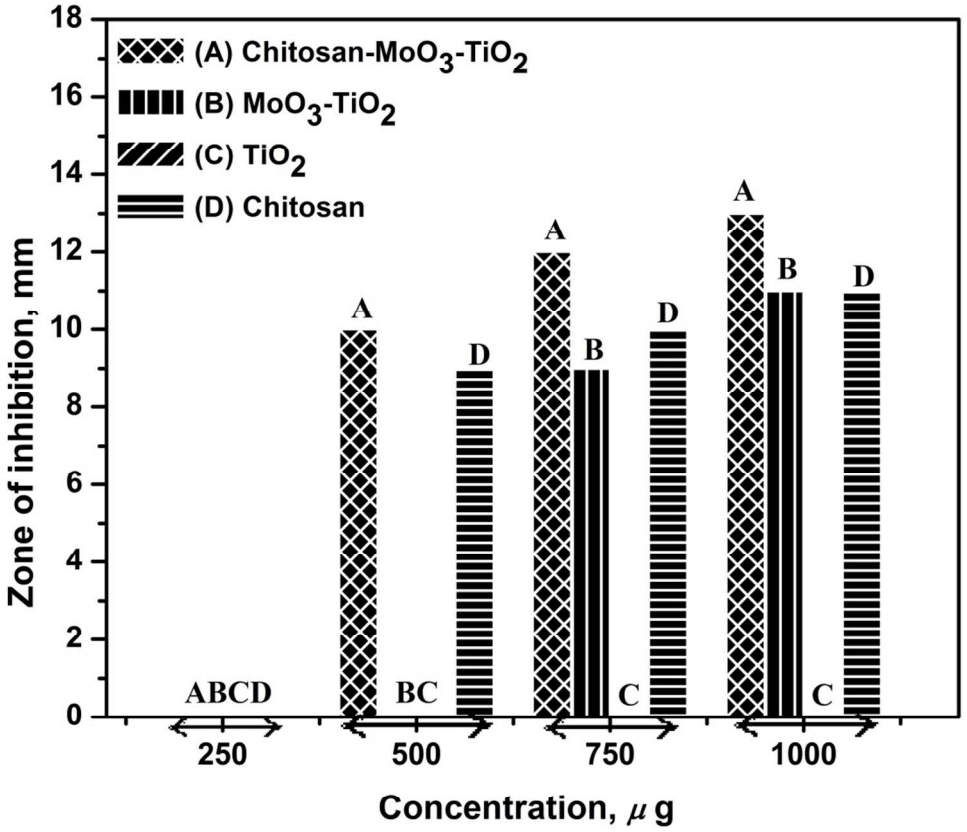

Fig. 10. Comparative study of the zone of inhibition (mm) for (A) Chitosan-blended MoO_3-TiO_2, (B) MoO_3-TiO_2, (C) TiO_2 and (D) Chitosan film in *E. coli* bacterial strain

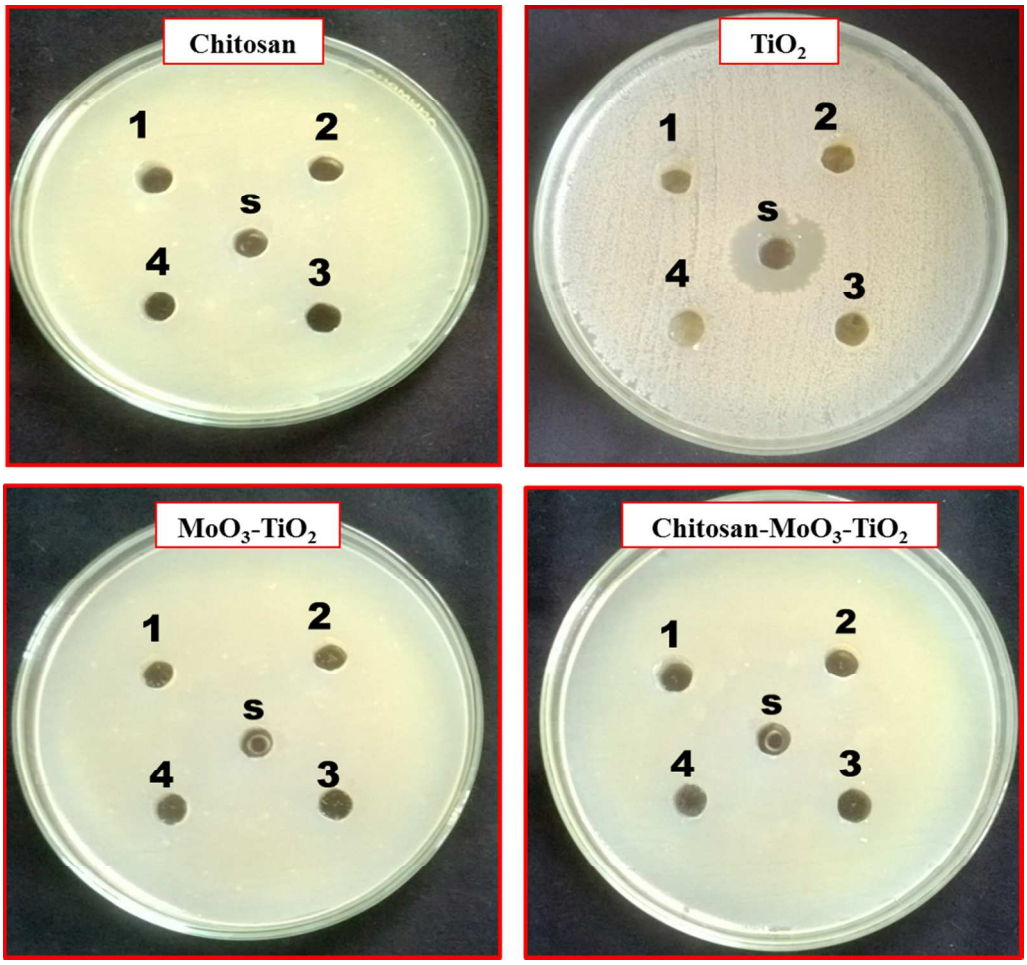

Fig. 11. Well diffusion assay of Chitosan, TiO_2, MoO_3-TiO_2 and Chitosan-blended MoO_3-TiO_2 nanocomposites

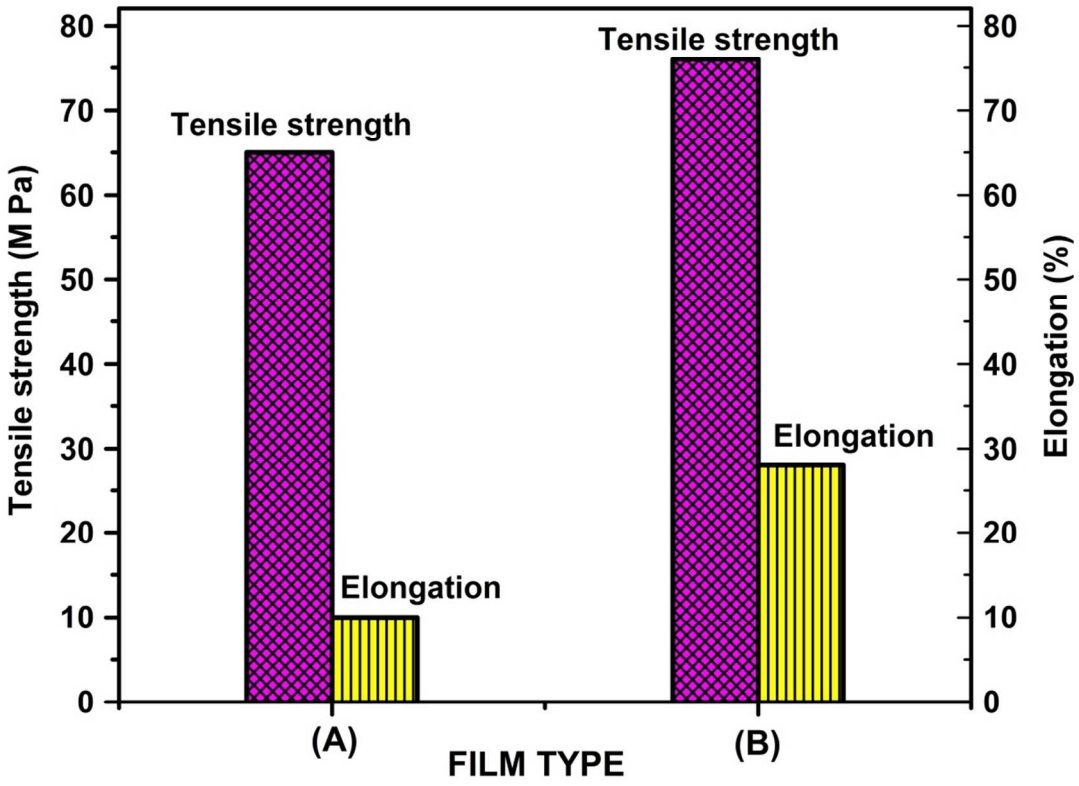

Fig. 12. Mechanical properties of (A) Chitosan and (B) Chitosan-blended MoO_3-TiO_2 film

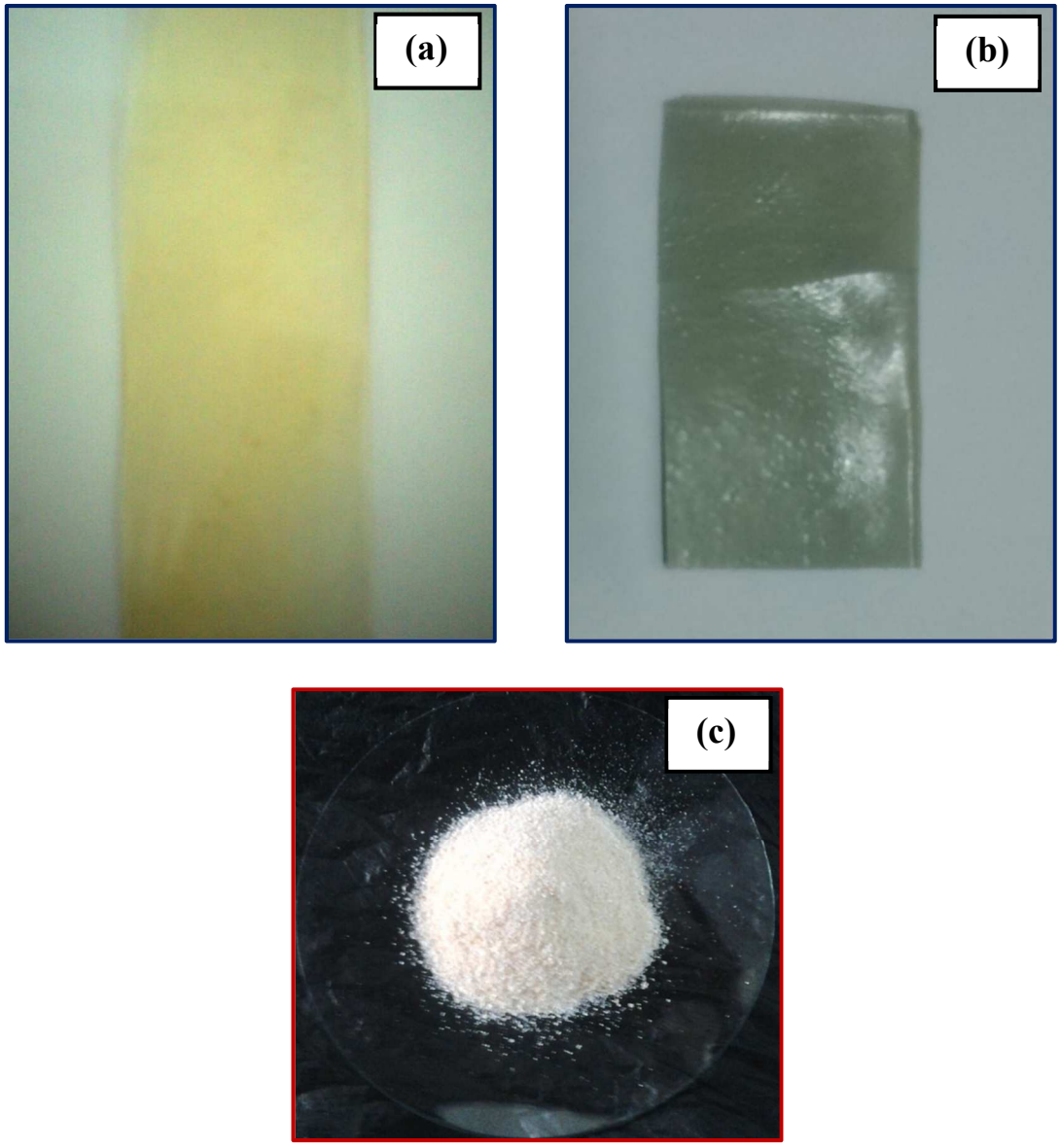

Fig. 13 . Photographs of (a) Chitosan film, (b) Chitosan-blended MoO_3-TiO_2 film and (c) Chitosan powder

NOVEL HYBRID CHITOSAN BLENDED MoO_3-TiO_2 NANOCOMPOSITE FILM: EVALUATION OF ITS SOLAR LIGHT PHOTOCATLYTIC AND ANTIBACTERIAL ACTIVITY

P. Magesan, S. Sanuja and M. J. Umapathy*

***Corresponding author: Department of Chemistry, College of Engineering Guindy Campus, AnnaUniversity, Chennai - 25, India.**

Graphical Abstract